Optics & Laser Technology 140 (2021) 107030

Contents lists available at ScienceDirect

Optics and Laser Technology

journal homepage: www.elsevier.com/locate/optlastec

Full length article

Waveguides fabrication by femtosecond laser in Tb^{3+}/Yb^{3+} doped CaLiBO glasses

S.N.C. Santos [a,*], G.F.B. Almeida [b], J.M.P. Almeida [a,c], A.C. Hernandes [a], C.R. Mendonça [a,*]

[a] São Carlos Institute of Physics, University of São Paulo, PO Box 369, 13560-970 São Carlos, SP, Brazil
[b] Institute of Physics, Federal University of Uberlândia, PO Box 593, 38400-902 Uberlândia, MG, Brazil
[c] Department of Materials Engineering, São Carlos School of Engineering, University of São Paulo, Av. João Dagnone, 1100, 13563-120 São Carlos, SP, Brazil

ARTICLE INFO

Keywords:
CaLiBO glasses
Femtosecond laser micromachining
Glass waveguides
Rare earths
Tb^{3+} - Yb^{3+} ions

ABSTRACT

Borate glasses present the ability to host various modifier ions and, therefore, are adaptable for a wide range of applications. Specifically, calcium-lithium tetraborate (CaLiBO) glasses doped with rare earths have been investigated for applications involving energy transfer processes. In this work, waveguides were inscribed by femtosecond laser microfabrication in CaLiBO glasses containing Tb^{3+} and Yb^{3+} ions, displaying emission in the green region. Single-mode guiding at 632.8 nm, with propagation losses of approximately 2.0 dB/cm, was obtained in 7.0-mm long waveguides with a diameter on the order of 2 μm, produced in the glass bulk, at approximately 100 μm below the sample surface. By coupling 488 nm light, the fabricated waveguide showed the capability of guiding the typical emission of Tb^{3+} ions. Such glasses containing rare earths could be suitable for the development of green light-emitting microdevices.

1. Introduction

Boron oxide is a relevant compound for glass technology not only by its ability to form a vitreous network on its own, but also due to its processing features, including low melting point and good solubility of the oxide modifiers and rare earth ions [1]. Notably, CaLiBO glass (calcium-lithium tetraborate glass) doped with rare earth elements has been considered a luminescent matrix suitable for energy transfer [2–4]. In general, rare earth ions exhibit luminescence from the visible to the infrared region in several types of materials [5–9]. Among the rare-earth ions, Tb^{3+} presents blue and green emission under UV excitation, which has motivated studies for its applications as the gain medium for green lasers and white light-emitting devices [10–13]. Glasses containing Yb^{3+} exhibit near-infrared absorption, a feature that makes them appropriate for diode lasers pumping. Also, their broad-band emission, from 900 to 980 nm, makes them suitable for generating ultrashort laser pulses, aiming applications that include solid-state lasers, up-conversion, and down-conversion processes [14]. Mutual use of Tb^{3+} and Yb^{3+} showed to be suitable for use in solar cells [15–17] and green fiber laser [18,19]. CaLiBO glasses containing Tb^{3+} and Yb^{3+} presented down-conversion in the near-infrared region and are potentially interesting materials for use solar cells [20]. Regarding its processing, femtosecond laser writing has already proven to be an important tool for the micromachining of glassy materials, targeting applications such as waveguides and lab-on-a-chip systems [21,22]. Since its first demonstration by Davis et al. in 1996 [23], femtosecond laser writing has been shown to be effective for waveguides production due to its capability to induce in the focal volume, a permanent change in the refractive index through nonlinear optical interactions [24]. Several works have reported the production of type I waveguides in rare-earth-doped glasses [25–34]. According to the type of change induced in the refractive index, waveguides produced in the bulk of materials can be classified into three categories. Type I modification occurs when there is an increase in the refractive index in the region irradiated by the laser. The double-line waveguide is known as type II modification; this configuration is composed of two parallel tracks that present a reduced refractive index. Besides, the tracks have an appropriate separation that delimits the confinement of light. The Type III modification, known as the cladding waveguide, consists of several near tracks with a low refractive index, while the core involved in these tracks has a high refractive index. Thus, the tracks act as cladding, and light confinement is observed in the core [35]. Also planar and ridge waveguides have been obtained through the combination of ion implantation and fs-laser processing, which has also been demonstrate in magneto-optical glasses [36–38].

* Corresponding authors.
E-mail addresses: ncs.sabrina@gmail.com (S.N.C. Santos), crmendon@ifsc.usp.br (C.R. Mendonça).

https://doi.org/10.1016/j.optlastec.2021.107030
Received 21 November 2020; Received in revised form 28 January 2021; Accepted 19 February 2021
Available online 26 February 2021

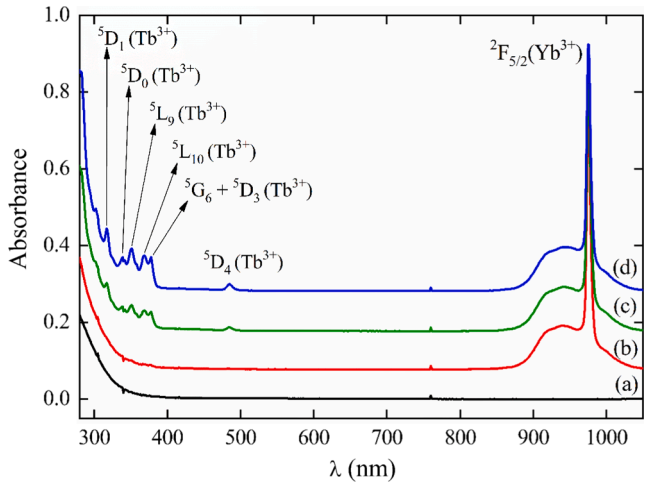

Fig. 1. The absorption spectra of samples CaLiBO (a), CaLiBOx01 (b), CaLiBOx1 (c) and CaLiBOx2 (d) showing the absorption bands of Tb^{3+} and Yb^{3+}. Each curve was shifted in the y-axis to better visualization.

In this work, motivated by the luminescent properties of Tb^{3+} and Yb^{3+} ions added in the CaLiBO glass system [20], we studied the femtosecond laser fabrication of inscribed waveguides in the volume of such glass system. The produced waveguides presented homogeneity along their length with cross-section sizing approximately 2 μm. The waveguides show propagation losses on the order of 2 dB/cm at 632.8 nm. Upon coupling light at the appropriate wavelength, it was possible to observe the waveguiding of the green Tb^{3+} emission, which can be used for active optical elements.

2. Experimental

The glass system studied here is composed by (99-x) CaLiBO + $1Yb_2O_3$ + xTb_4O_7 with x = 0.1, 1.0 and 2.0 (mol%), designated as CaLiBOx01, CaLiBOx1 and CaLiBOx2. CaLiBO matrix contain $60B_2O_3$ + 30CaO + $10Li_2O$ (mol%). All samples were prepared by the melt-quenching technique, using platinum crucible and high purity oxides or carbonates (B_2O_3 - Alfa Aesar 97,5%; Li_2CO_3 - Carlo Erba 99%; $CaCO_3$ - Alfa Aesar 99,5%; Tb_4O_7 - Alfa Aesar 99,9%; and Yb_2O_3 - Alfa Aesar 99,9%), as described in Ref. [39].

Femtosecond laser writing was performed with an extended cavity Ti:sapphire laser oscillator centered at 800 nm, with a maximum pulse energy of 100 nJ, delivering 50-fs pulses and operating at a repetition rate of 5 MHz. High repetition rates (HRR) operate in a thermal regime, allowing heat accumulation around the focal volume. Some studies have shown that the combination of HRR and heat accumulation enables the production of structures with symmetric cross-sections and reduces coupling and propagation losses [40–42]. It is worth mentioning that different combinations of glass systems and laser systems can originate waveguides with distinct features.

Ultrashort pulses were focused by a microscope objective (NA = 0.65) within the sample. Simultaneously, the sample was moved perpendicularly to the laser beam by a translational *xyz* stage moved at 10, 50, and 200 μm/s. We determined the guiding properties of the produced waveguides by using an objective-lens-based coupling system [43]; standard (NA = 0.40 and 0.17) and UV-coated microscopy objectives (NA = 0.40 and 0.50) were used to couple light from HeNe laser (632.8 nm) and Argon ion laser (488 nm), respectively. We observed the guided modes with a CCD camera. Waveguide total losses, including Fresnel reflection, coupling, and propagation losses, were determined by measuring the laser power at the waveguide input and output [43]. Coupling losses were determined by the mode-mismatch between the guided mode profile and the input Gaussian laser beam, according to the method described in Ref. [27,44]. We estimated the Fresnel losses by using the index of refraction of the glasses. Thus, we obtained propagation losses by discounting Fresnel and coupling losses from the measured total loss.

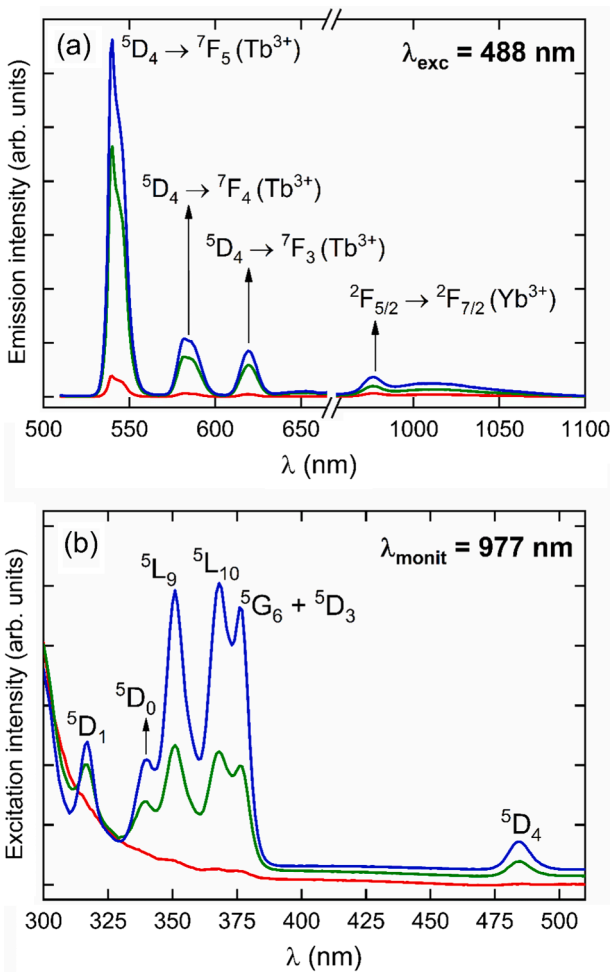

Fig. 2. (a) Emission spectrum with excitation at 488 nm and (b) excitation spectrum monitored at 977 nm for CaLiBOx01 (red curve), CaLiBOx1 (green curve), and CaLiBOx2 (blue curve).

3. Results and discussion

Fig. 1 shows the absorption spectrum of CaLiBO (a), CaLiBOx01 (b), CaLiBOx1 (c), and CaLiBOx2 (d). As one can see, the CaLiBO sample is transparent for wavelengths over 350 nm. The samples containing the rare earth elements present the characteristics of absorption bands of Tb^{3+} and Yb^{3+} [45]. For Tb^{3+}, six absorption bands, related to electronic transitions from the ground state ($^7F_6$) to excited states, can be identified; at 317 nm ($^5D_1$), 338 nm ($^5D_0$), 350 nm ($^5L_9$), 368 nm ($^5L_{10}$), 377 nm ($^5G_6$ + $^5D_3$) and 484 nm ($^5D_4$) [12,46]. For Yb^{3+}, one absorption band from the ground state ($^2F_{7/2}$) can be identified at 975 nm ($^2F_{5/2}$) [47]. An increase in the Tb^{3+} absorption bands corresponding to the concentration of this ion according to x = 0.1, 1.0 and 2.0 in the system (99 - x)% CaLiBO + $1\%Yb_2O_3$ + $x\%Tb_4O_7$, is observed.

The emission spectrum of the rare earth doped samples is shown in Fig. 2(a) when excited at 488 nm. Such results show the emission bands corresponding to Tb^{3+} in the visible spectral region, at 547 nm ($^5D_4 \rightarrow {}^7F_5$), 588 nm ($^5D_4 \rightarrow {}^7F_4$), and 624 nm ($^5D_4 \rightarrow {}^7F_3$). The emission band of Yb^{3+} is present in the near-infrared region at 977 nm ($^2F_{5/2} \rightarrow {}^2F_{7/2}$). Fig. 2(b) displays the excitation spectrum when monitoring the Yb^{3+} emission at 977 nm. As can be seen, the excitation spectrum is similar to the absorption spectrum of the Tb^{3+}, as shown in Fig. 1. This result

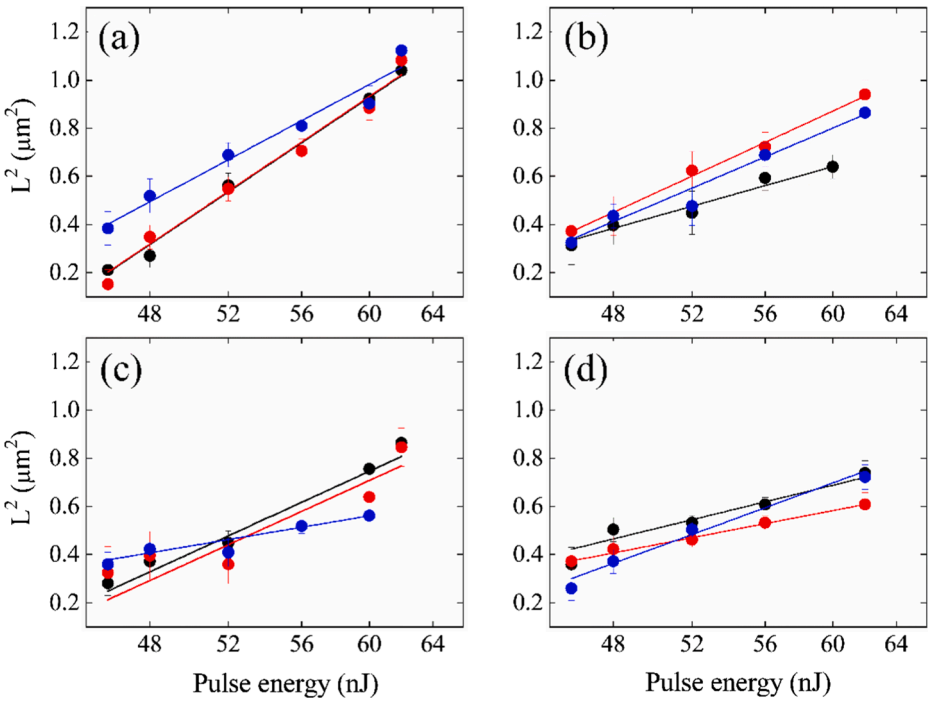

Fig. 3. Squared line width (L^2) as a function of the pulse energy (log scale) for CaLiBO (a), CaLiBOx01 (b), CaLiBOx1 (c), and CaLiBOx2 (d) for three translation speeds 10 μm/s (black circles), 50 μm/s (red circles), and 200 μm/s (blue circles).

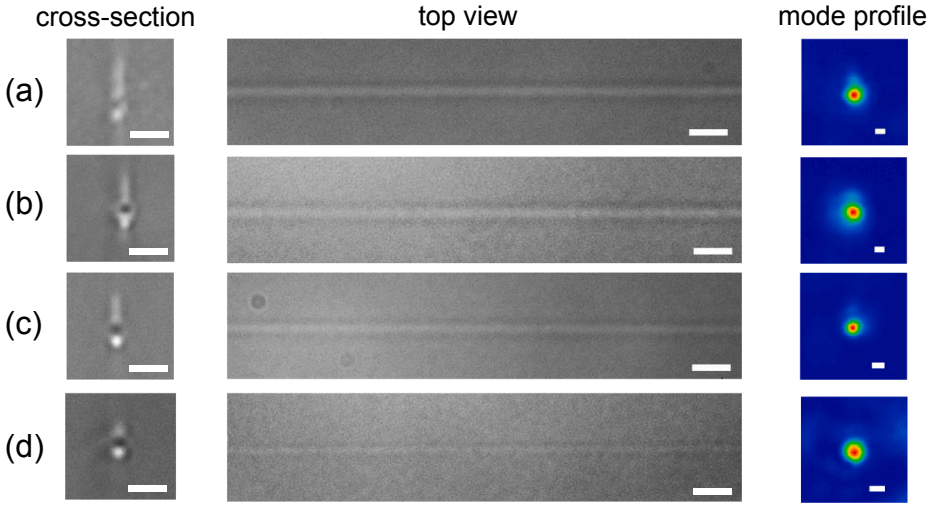

Fig. 4. Optical microscopy images (cross-section view of the input face and top view) of waveguides produced in the glass system, along with the near-field output profile (mode profile) of light guided at 632.8 nm. For samples CaLiBO (a), CaLiBOx01 (b) and CaLiBOx1 (c). Scale bar in each image corresponds to 5 μm.

indicates the down-conversion process from Tb^{3+} to Yb^{3+} [20] since glass systems co-doped with Tb^{3+} and Yb^{3+} ions are known to exhibit the energy transfer process of down-conversion [48–50].

Before carrying out the fabrication of the waveguides, we performed a study on the fs-laser micromachining condition on the CaLiBO samples, varying the pulse energy and the scanning speed to determine the threshold energy (E_{th}), which represents the minimum energy to modify the sample. Fig. 3 shows the dependence of the line width squared (L^2), produced by fs-laser micromachining, as a function of the pulse energy (log–scale). The line width values in all samples increase with pulse energy, varying from approximately 0.4–1.08 μm when the pulse energy increases from 46 to 62 nJ, for the scanning speeds of 10, 50, and 200 μm/s. By fitting the data shown in Fig. 3 using the model presented in Ref. [51], we determined the threshold energies (E_{th}), which are in the range of about 30–42 nJ.

Fig. 4 shows optical microscopy images of the top (a) and cross-section (b) views of waveguides produced by fs-laser micromachining in the CaLiBO glasses systems studied here. The waveguides are 7.0-mm long (sample size limitation) and were produced approximately 100 μm below the sample surface. For the production of waveguides with good optical quality and homogeneity, and pulse energies used for the fabrication were 46 nJ for CaLiBO, 48 nJ for sample CaLiBOx01, and 52 nJ for samples CaLiBOx1 and CaLiBOx2 at the scanning speeds of 200 μm/s for all samples. Fig. 4 displays optical microscopy images of the cross-section and top view of some waveguides, revealing that the waveguides are homogeneous along their length and exhibit slightly elliptical cross-sections with dimensions on the order of ~2 μm. Also, the near-field output profile shown in Fig. 4 indicates a monomode operation

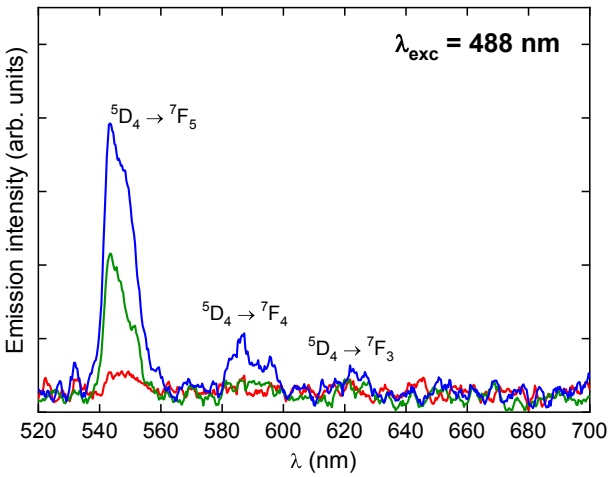

Fig. 5. Emission spectra obtained at the waveguides output when coupling light at 488 nm to CaLiBOx01 (red line), CaLiBOx1 (green line) and CaLiBOx2 (blue line).

of the fabricate waveguides at 632.8 nm.

The mode profile of the waveguides at 632.8 nm, as shown in Fig. 4 (c), indicates single-mode operation. By adjusting such intensity distribution assuming the fundamental mode of a step-index waveguide, a refractive index change on the order of 1.0×10^{-3} was determined for all samples, in agreement with other results reported in the literature [25,52].

The values obtained for the propagation loss are (1.8 ± 0.6), (1.9 ± 0.8), (1.8 ± 0.6) and (1.7 ± 0.7) dB/cm for the CaLiBO, CaLiBOx01, CaLiBOx1, CaLiBOx2 samples, respectively, which is in agreement with other results reported for micromachined waveguides produced by different fs-laser and vitreous systems [29,33,34,53]. Fig. 5 displays the spectra of the emission bands, which correspond to the emission of Tb^{3+}, which is in agreement with the spectrum present in Fig. 2 (a), although it presents a smaller signal to noise ration. Such results indicate that the micromachining does not change the emission properties of the samples. The emission band corresponding to the Yb^{3+} ion (at 977 nm) was not observed at the output of the waveguide because it is below our detection limit, given its small relative intensity, as can be seen in Fig. 2(a). Also, the low Yb^{3+} content in the sample, as well as insufficient excitation intensity may also make it difficult to observe such band.

In order to collect only the guided emission, a filter was used to block the wavelength of the coupled excitation. In this way, the glasses investigated herein are favorable candidates for devices that emit green light since they can host waveguide capable of guiding its own fluorescent emission.

4. Conclusions

This work showed the inscription of homogeneous waveguides in the CaLiBO glass system doped with Tb^{3+} and Yb^{3+} via femtosecond direct laser writing. We found that the best experimental conditions to write waveguides with optimal optical quality on the samples investigated here is pulse energy ranged 46–52 nJ with scanning speed of 200 μm/s. In addition, the waveguides are capable of supporting single mode guiding when coupled at 632.8 nm. The characterization of waveguides at 632.8 nm, reported a refractive index change on the order of 1.0×10^{-3}, leading to a propagation loss of approximately 2 dB/cm for CaLiBO glass system. Finally, these doped waveguides are able to guide the emission of the Tb^{3+}, resulting in an optical device with visible emission in green. The intensity of emission can be managed by the Tb^{3+} content, in which its increase up to 2 mol% improved the fluorescence and guiding of green light, without changing the waveguide loss or fabrication condition.

CRediT authorship contribution statement

S.N.C. Santos: Conceptualization, Methodology, Validation, Formal analysis, Investigation, Writing - original draft, Writing - review & editing, Visualization. **G.F.B. Almeida:** Methodology, Software, Validation, Formal analysis, Writing - review & editing. **J.M.P. Almeida:** Methodology, Resources, Writing - review & editing. **A.C. Hernandes:** Resources, Writing - review & editing. **C.R. Mendonca:** Conceptualization, Methodology, Validation, Investigation, Resources, Writing - review & editing, Visualization, Supervision, Project administration, Funding acquisition.

Declaration of Competing Interest

The authors declare that they have no known competing financial interests or personal relationships that could have appeared to influence the work reported in this paper.

Acknowledgments

The authors gratefully acknowledge the financial support from the Coordenação de Aperfeiçoamento de Pessoal de Nível Superior (CAPES) - Finance Code 001, CNPq and FAPESP (2018/11283-7). The authors also thank André Luis dos Santos Romero for technical assistance.

References

[1] F. Steudel, A.C. Rimbach, S. Loos, B. Ahrens, S. Schweizer, Effect of induced crystallization in rare-earth doped lithium borate glass, Radiat. Meas. 90 (2016) 274–278, https://doi.org/10.1016/j.radmeas.2015.12.046.

[2] J.C. Joshi, B.C. Joshi, N.C. Pandey, R. Belwal, J. Joshi, Nonradiative energy transfer from $Tb^{3+} \rightarrow Er^{3+}$ in calibo glass, J. Solid State Chem. 22 (1977) 439–443, https://doi.org/10.1016/0022-4596(77)90021-4.

[3] J.C. Joshi, N.C. Pandey, B.C. Joshi, R. Belwal, J. Joshi, Diffusion limited energy transfer from $Tb^{3+} \rightarrow Ho^{3+}$ in CALIBO glass, J. Non. Cryst. Solids. 27 (1978) 173–179, https://doi.org/10.1016/0022-3093(78)90121-7.

[4] G. Tripathi, V.K. Rai, S.B. Rai, Optical properties of Sm^{3+}:CaO-Li2O-B_2O_3-BaO glass and codoped Sm^{3+}:Eu^{3+}, Appl. Phys. B. 84 (2006) 459–464, https://doi.org/10.1007/s00340-006-2239-5.

[5] E.B. Gibelli, J. Kai, E.E.S. Teotonio, O.L. Malta, M.C.F.C. Felinto, H.F. Brito, Photoluminescent PMMA polymer films doped with Eu^{3+} -β-diketonate crown ether complex, J. Photochem. Photobiol. A Chem. 251 (2013) 154–159, https://doi.org/10.1016/j.jphotochem.2012.10.015.

[6] H.S. Santos, T. Laihinen, L.C.V. Rodrigues, J. Sinkkonen, E. Mäkilä, P. Damlin, L.K. O. Nakamura, H.F. Brito, J. Hölsä, M. Lastusaari, Red- and green-emitting nanoclay materials doped with Eu^{3+} and/or Tb^{3+}, Luminescence. 34 (2019) 23–38, https://doi.org/10.1002/bio.3561.

[7] A. Sas-Bieniarz, B. Marczewska, M. Kłosowski, P. Bilski, W. Gieszczyk, TL, OSL and RL emission spectra of RE-doped $LiMgPO_4$ crystals, J. Lumin. 218 (2020), https://doi.org/10.1016/j.jlumin.2019.116839.

[8] N. Wantana, E. Kaewnuam, B. Damdee, S. Kaewjaeng, S. Kothan, H.J. Kim, J. Kaewkhao, Energy transfer based emission analysis of Eu^{3+} doped Gd_2O_3-CaO-SiO_2-B_2O_3 glasses for laser and X-rays detection material applications, J. Lumin. 194 (2018) 75–81, https://doi.org/10.1016/j.jlumin.2017.10.004.

[9] L. Ruiyi, L. Zaijun, S. Xiulan, J. Jan, L. Lin, G. Zhiguo, W. Guangli, Graphene quantum dot-rare earth upconversion nanocages with extremely high efficiency of upconversion luminescence, stability and drug loading towards controlled delivery and cancer theranostics, Chem. Eng. J. 382 (2020) 1–13, https://doi.org/10.1016/j.cej.2019.122992.

[10] J.K. Cao, W.P. Chen, L.P. Chen, X.Y. Sun, H. Guo, Synthesis and characterization of $BaLuF_5$: Tb^{3+} oxyfluoride glass ceramics as nanocomposite scintillator for X-ray imaging, Ceram. Int. 42 (2016) 17834–17838, https://doi.org/10.1016/j.ceramint.2016.08.114.

[11] V.S. Kavitha, R. Reshmi Krishnan, R. Sreeja Sreedharan, K. Suresh, C. K. Jayasankar, V.P. Mahadevan Pillai, Tb^{3+} -doped WO_3 thin films: a potential candidate in white light emitting devices, J. Alloys Compd. 788 (2019) 429–445, https://doi.org/10.1016/j.jallcom.2019.02.222.

[12] S.N.S. Yaacob, M.R. Sahar, E.S. Sazali, Z.A. Mahraz, K. Sulhadi, Comprehensive study on compositional modification of Tb^{3+} doped zinc phosphate glass, Solid State Sci. 81 (2018) 51–57, https://doi.org/10.1016/j.solidstatesciences.2018.05.006.

[13] J. Juárez-Batalla, A.N. Meza-Rocha, G.H. Muñoz, I. Camarillo, U. Caldiño, Luminescence properties of Tb^{3+}-doped zinc phosphate glasses for green laser application, Opt. Mater. (Amst) 58 (2016) 406–411, https://doi.org/10.1016/j.optmat.2016.06.022.

[14] K.V. Krishnaiah, E.S. De Lima Filho, Y. Ledemi, G. Nemova, Y. Messaddeq, R. Kashyap, Development of ytterbium-doped oxyfluoride glasses for laser cooling applications, Sci. Rep. 6 (2016) 1–12, https://doi.org/10.1038/srep21905.

[15] A. Bahadur, R.S. Yadav, R.V. Yadav, S.B. Rai, Multimodal emissions from Tb^{3+}/Yb^{3+}co-doped lithium borate glass: upconversion, downshifting and quantum cutting, J. Solid State Chem. 246 (2017) 81–86, https://doi.org/10.1016/j.jssc.2016.11.004.

[16] M. Isogai, T. Hayakawa, J.-R. Duclère, P. Thomas, Quantum cutting properties of Tb^{3+}/Yb^{3+} co-doped ZrO_2 -SiO_2 nano-crystalized glasses synthesized via a sol-gel route, J. Alloys Compd. 781 (2019) 315–320, https://doi.org/10.1016/j.jallcom.2018.11.380.

[17] I.-S. Yu, S.-C. Wu, L. Dumont, J. Cardin, C. Labbé, F. Gourbilleau, Monolithic crystalline silicon solar cells with SiNx layers doped with Tb^{3+} and Yb^{3+} rare-earth ions, J. Rare Earths. 37 (2019) 515–519, https://doi.org/10.1016/j.jre.2018.07.014.

[18] A. Lin, X. Liu, P.R. Watekar, H. Guo, B. Peng, W. Wei, M. Lu, W.T. Han, J. Toulouse, Intense green upconversion emission in Tb^{3+}/Yb^{3+} codoped alumino-germano-silicate optical fibers, Appl. Opt. 49 (2010) 1671–1675, https://doi.org/10.1364/AO.49.001671.

[19] Z. Zhou, A. Lin, H. Guo, X. Liu, C. Hou, M. Lu, W. Wei, B. Peng, W. Zhao, J. Toulouse, Tb^{3+}/Yb^{3+} heavily-doped tellurite glasses with efficient green light emission, J. Non. Cryst. Solids. 356 (2010) 2896–2899, https://doi.org/10.1016/j.jnoncrysol.2010.09.010.

[20] I.A.A. Terra, L.J. Borrero-González, T.R. Figueredo, J.M.P. Almeida, A. C. Hernandes, L.A.O. Nunes, O.L. Malta, Down-conversion process in Tb^{3+} Yb^{3+} co-doped Calibo glasses, J. Lumin. 132 (2012) 1678–1682, https://doi.org/10.1016/j.jlumin.2012.02.019.

[21] M. Khalid, G.Y. Chen, J. Bei, H. Ebendorff-Heidepriem, D.G. Lancaster, Microchip and ultra-fast laser inscribed waveguide lasers in Yb^{3+} germanate glass, Opt. Mater. Express. 9 (2019) 3557–3564, https://doi.org/10.1364/ome.9.003557.

[22] F. Sima, K. Sugioka, R.M. Vázquez, R. Osellame, L. Kelemen, P. Ormos, Three-dimensional femtosecond laser processing for lab-on-a-chip applications, Nanophotonics. 7 (2018) 613–634, https://doi.org/10.1515/nanoph-2017-0097.

[23] K.M. Davis, K. Miura, N. Sugimoto, K. Hirao, Writing waveguides in glass with a femtosecond laser, Opt. Lett. 21 (1996) 1729–1731.

[24] R.R. Gattass, E. Mazur, Femtosecond laser micromachining in transparent materials, Nat. Photonics. 2 (2008) 219–225, https://doi.org/10.1038/nphoton.2008.47.

[25] N.D. Psaila, R.R. Thomson, H.T. Bookey, A.K. Kar, N. Chiodo, R. Osellame, G. Cerullo, A. Jha, S. Shen, Er:Yb-doped oxyfluoride silicate glass waveguide amplifier fabricated using femtosecond laser inscription, Appl. Phys. Lett. 90 (2007) 90–93, https://doi.org/10.1063/1.2716866.

[26] L.B. Fletcher, J.J. Witcher, N. Troy, S.T. Reis, R.K. Brow, D.M. Krol, L.B. Fletcher, J. J. Witcher, N. Troy, S.T. Reis, R.K. Brow, D.M. Krol, Effects of rare-earth doping on femtosecond laser waveguide writing in zinc polyphosphate glass, J. Appl. Phys. 112 (2012), https://doi.org/10.1063/1.4739288.

[27] R. Osellame, N. Chiodo, G. Valle, S. Taccheo, R. Ramponi, G. Cerullo, A. Killi, U. Morgner, M. Lederer, D. Kopf, Optical waveguide writing with a diode-pumped femtosecond oscillator, Opt. Lett. 29 (2004) 1900–1902, https://doi.org/10.1364/OL.29.001900.

[28] R. Osellame, S. Taccheo, G. Cerullo, M. Marangoni, D. Polli, R. Ramponi, P. Laporta, S. De Silvestri, Optical gain in Er-Yb doped waveguides fabricated by femtosecond laser pulses, Electron. Lett. 38 (2002) 964–965, https://doi.org/10.1049/el:20020649.

[29] R.R. Thomson, H.T. Bookey, N. Psaila, S. Campbell, D.T. Reid, S. Shen, A. Jha, A. K. Kar, Internal gain from an erbium-doped oxyfluoride-silicate glass waveguide fabricated using femtosecond waveguide inscription, IEEE Photonics Technol. Lett. 18 (2006) 1515–1517.

[30] P. Nandi, G. Jose, C. Jayakrishnan, S. Debbarma, K. Chalapathi, K. Alti, A. K. Dharmadhikari, J.A. Dharmadhikari, D. Mathur, Femtosecond laser written channel waveguides in tellurite glass, Opt. Express. 14 (2006) 12145, https://doi.org/10.1364/oe.14.012145.

[31] T. Toney Fernandez, G. Della Valle, R. Osellame, G. Jose, N. Chiodo, A. Jha, P. Laporta, Active waveguides written by femtosecond laser irradiation in an erbium-doped phospho-tellurite glass, Opt. Express. 16 (2008) 15198–15205.

[32] Y. Duan, P. Dekker, M. Ams, G. Palmer, M.J. Withford, Time dependent study of femtosecond laser written waveguide lasers in Yb-doped silicate and phosphate glass, Opt. Mater. Express. 5 (2015) 416, https://doi.org/10.1364/ome.5.000416.

[33] A. Dias, F. Muñoz, A. Alvarez, P. Moreno-Zárate, J. Atienzar, A. Urbieta, P. Fernandez, M. Pardo, R. Serna, J. Solis, Femtosecond laser writing of photonic devices in borate glasses compositionally designed to be laser writable, Opt. Lett. 43 (2018) 2523, https://doi.org/10.1364/ol.43.002523.

[34] S.N.C. Santos, J.M.P. Almeida, G.F.B. Almeida, V.R. Mastelaro, C.R. Mendonca, Fabrication of waveguides by fs-laser micromachining in Dy^{3+}/Eu^{3+} doped barium borate glass with broad emission in the visible spectrum, Opt. Commun. 427 (2018) 33–36, https://doi.org/10.1016/j.optcom.2018.06.026.

[35] F. Chen, J.R.V. de Aldana, Optical waveguides in crystalline dielectric materials produced by femtosecond-laser micromachining, Laser Photon. Rev. 8 (2014) 251–275, https://doi.org/10.1002/lpor.201300025.

[36] J.-Y. Chen, J. Zhang, L.L. Zhang, C.-X. Liu, Fabrication of ridge waveguide on the ion-implanted TGG crystal by femtosecond laser ablation, J. Mod. Opt. 67 (2020) 1100–1104, https://doi.org/10.1080/09500340.2020.1810795.

[37] J. Zhang, Y. Zhang, J. Xu, S.-B. Lin, C.-X. Liu, Planar and ridge waveguides formed by proton implantation and femtosecond laser ablation in fused silica, Vacuum. 172 (2020), 109093, https://doi.org/10.1016/j.vacuum.2019.109093.

[38] Q.F. Zhu, Y. Wang, X.L. Shen, H.T. Guo, C.X. Liu, Optical ridge waveguides in magneto-optical glasses fabricated by combination of silicon ion implantation and femtosecond laser ablation, IEEE Photonics J. 10 (2018) 1–7, https://doi.org/10.1109/JPHOT.2018.2867491.

[39] S.N.C. Santos, K.T. Paula, J.M.P. Almeida, A.C. Hernandes, C.R. Mendonça, Effect of Tb^{3+}/Yb^{3+} in the nonlinear refractive spectrum of CaLiBO glasses, J. Non. Cryst. Solids. 524 (2019) 1–5, https://doi.org/10.1016/j.jnoncrysol.2019.119637.

[40] S.M. Eaton, H. Zhang, M.L. Ng, J. Li, W.-J. Chen, S. Ho, P.R. Herman, Transition from thermal diffusion to heat accumulation in high repetition rate femtosecond laser writing of buried optical waveguides, Opt. Express. 16 (2008) 9443, https://doi.org/10.1364/oe.16.009443.

[41] B. McMillen, K.P. Chen, D. Jaque, Microstructural imaging of high repetition rate ultrafast laser written $LiTaO_3$ waveguides, Appl. Phys. Lett. 94 (2009) 111–114, https://doi.org/10.1063/1.3088852.

[42] C.B. Schaffer, J.F. García, E. Mazur, Bulk heating of transparent materials using a high-repetition-rate femtosecond laser, Appl. Phys. A. A 76 (2003) 351–354, https://doi.org/10.1007/s00339-002-1819-4.

[43] J.M.P. Almeida, P.H.D. Ferreira, D. Manzani, M. Napoli, S.J.L. Ribeiro, C. R. Mendonça, Metallic nanoparticles grown in the core of femtosecond laser micromachined waveguides, J. Appl. Phys. 193507 (2014) 1–6, https://doi.org/10.1063/1.4875485.

[44] R. Osellame, G. Cerullo, R. Ramponi, Femtosecond Laser Micromachining: Photonic and Microfluidic Devices in Transparent Materials, Springer-Verlag GmbH, 2012 https://doi.org/10.1007/978-3-642-23366-1.

[45] I.A.A. Terra, L.J. Borrero-González, J.M.P. Almeida, A.C. Hernandes, L.A.O. Nunes, Judd-Ofelt analysis of Tb^{3+} and upconversion study in Yb^{3+}–Tb^{3+} co-doped calibo glasses, Quim. Nova. 43 (2020) 188–193, https://doi.org/10.21577/0100-4042.20170465.

[46] K. Linganna, J. S, B. Ch, V. Venkatramu, C.K. Jayasankar, Luminescence and decay characteristics of Tb3+-doped fluorophosphate glasses, J. Asian Ceram. Soc. 6 (2018) 82–87. https://doi.org/10.1080/21870764.2018.1442674.

[47] S. Wang, F. Lou, C. Yu, Q. Zhou, M. Wang, S. Feng, D. Chen, L. Hu, W. Chen, M. Guzik, G. Boulon, Influence of Al^{3+} and P^{5+} ion contents on the valence state of Yb^{3+} ions and the dispersion effect of Al^{3+} and P^{5+} ions on Yb^{3+} ions in silica glass, J. Mater. Chem. C. 2 (2014) 4406–4414, https://doi.org/10.1039/C3TC32576H.

[48] J. Hu, Y. Zhang, H. Xia, H. Ye, B. Chen, Y. Zhu, NIR downconversion and energy transfer mechanisms in Tb^{3+}/Yb^{3+} codoped $Na_5Lu_9F_{32}$ single crystals, Inorg. Chem. 57 (2018) 7792–7796, https://doi.org/10.1021/acs.inorgchem.8b00867.

[49] T. Grzyb, K. Kubasiewicz, A. Szczeszak, S. Lis, Energy migration in YBO_3:Yb^{3+}, T^{b3} + materials: down- and upconversion luminescence studies, J. Alloys Compd. 686 (2016) 951–961, https://doi.org/10.1016/j.jallcom.2016.06.230.

[50] B. Zheng, L. Lin, S. Xu, Z. Wang, Z. Feng, Z. Zheng, Efficient near-infrared downconversion and energy transfer mechanism in Tb^{4+}-Yb^{3+} co-doped $NaYF_4$ nanoparticles, Opt. Mater. Express. 6 (2016) 2769–2775, https://doi.org/10.1364/ome.6.002769.

[51] J.M. Liu, Simple technique for measurements of pulsed Gaussian-beam spot sizes, Opt. Lett. 7 (1982) 196, https://doi.org/10.1364/OL.7.000196.

[52] S. Thomas, T.T. Fernandez, J. Solis, P.R. Biju, N.V. Unnikrishnan, Optical channel waveguides written by high repetition rate femtosecond laser irradiation in Li–Zn fluoroborate glass, J. Opt. 47 (2018) 412–415, https://doi.org/10.1007/s12596-018-0462-1.

[53] J.M.P. Almeida, R.D. Fonseca, L. De Boni, A.R.S. Diniz, A.C. Hernandes, P.H. D. Ferreira, C.R. Mendonca, Waveguides and nonlinear index of refraction of borate glass doped with transition metals, Opt. Mater. (Amst) 42 (2015) 522–525, https://doi.org/10.1016/j.optmat.2015.01.048.